Supporting Information

Built-in electric fields in asymmetric carbon nitride nanotubes for improved solar biomass valorization and hydrogen generation

Xiang Zhong[†a], Yuxiang Zhu[†,*a], Yiyang Chen[a], Mengjiao Yu[a], Qiufan Sun[a], DongEn Zhang*[b], Yuhang Liang[c,d], Sai Xu[e] and Jianfeng Yao*[a]

[a] Jiangsu Co-Innovation Center of Efficient Processing and Utilization of Forest Resources, Jiangsu Province Key Laboratory of Green Biomass-based Fuels and Chemicals, College of Chemical Engineering, Nanjing Forestry University, Nanjing, Jiangsu, 210037, China.

[b] School of Environmental and Chemical Engineering, Jiangsu Ocean University, Lianyungang, 222005, China

[c] College of Chemistry, Fuzhou University, Fuzhou, Fujian, 350108, China.

[d] School of Physics, The University of Sydney, New South Wales, 2006, Australia.

[e] Jiangsu Key Laboratory of Chemical Pollution Control and Resources Reuse, School of Environmental and Biological Engineering, Nanjing University of Science and Technology, Nanjing, Jiangsu, 210094, China

[*]Corresponding author E-mail address: yxzhu89@njfu.edu.cn (Y. Zhu), zde@jou.edu.cn (D. Zhang), jfyao@njfu.edu.cn (J. Yao)

[†]The authors contributed equally to this work.

Supplementary Text

S1. Materials and reagents

All the chemicals used in this study were employed without further purification. Melamine was obtained from Shanghai Lingfeng Chemical Reagent Co., Ltd. Thiocarbohydrazide (TCH), 5-hydroxymethylfurfural (HMF) and 2-nitro-4-chlorophenol were purchased from Shanghai McLean Biochemical Technology Co., Ltd. 2,4,6-Triaminopyrimidine (TAP), acetonitrile, triethanolamine, and chloroplatinic acid hexahydrate were supplied by Shanghai Aladdin Biochemical Technology Co., Ltd. Urea, p-benzoquinone, glucose, ethylenediaminetetraacetic acid sodium and tert butanol were provided by Shanghai National Pharmaceutical Group Chemical Reagent Co., Ltd. High-purity argon gas (99.999%) was supplied by Nanjing Special Natural Gas Plant Co., Ltd.

S2. In situ diffuse reflectance infrared Fourier transform spectroscopy (DRIFTS) measurements

In situ DRIFTS measurements were performed using the Nicolet IZ10 spectrometer equipped with a Harrick in situ diffuse reflectance cell. The catalyst was held on the homemade sample table in the cell. Then, 50 μL aqueous solution of HMF (10 mM) was added to the catalyst. With continual Ar blowing into the cell for about 30 min, turn on the Xe lamp to irradiate the surface of the catalyst for 110 min. The spectra of the HMF adsorption on the catalyst under dark and light irradiation were recorded every 10 min.

S3. Density functional theory calculations

Density functional theory (DFT) calculations were conducted using Vienna Ab-initio Simulation Package (VASP) [1]. The interaction between core and valence electrons was characterized using the projector augmented wave (PAW) method [2]. The Perdew-Burke-Ernzerhof (PBE) functional, based on the generalized gradient approximation (GGA), was utilized to address the exchange and correlation potential [3]. A cutoff energy of 450 eV was employed with an energy convergence threshold of 1×10^{-5}

eV and a force convergence criterion of 0.02 eV/Å. A vacuum layer of 15 Å was introduced in the z-direction to prevent interactions between adjacent layers. A 2 × 2 × 1 k-point mesh for the Brillouin zone was utilized. The DFT-D3 method was also employed to describe the van der Waals interactions [4]. The hydrogen adsorption energy (ΔE_{H*}) was determined using the following formula:

$$\Delta E_{H*} = E_{H*} - E* - 1/2E_{H_2} \quad (1)$$

Where E_{H*}, E_*, E_{H2} denote the energy of the catalyst with an adsorbed hydrogen (H) atom, the energy of the catalyst, and the catalyst with a single H_2 molecule, respectively. The Gibbs free energy (ΔG_{H*}) for the H absorption was identified as:

$$\Delta G_{H*} = \Delta E_{H*} + \Delta ZPE - T\Delta S \quad (2)$$

Where ΔZPE represented the change in zero-point energy (ZPE) and ΔS denoted the entropy change (T = 298.15 K) between the adsorbed atomic hydrogen and the gaseous hydrogen.

S4. Electrochemical tests

Before the photoelectrochemical test, photoelectrodes were prepared using the dropping-drying method. Specifically, fluorine-doped tin oxide (FTO, 1 cm × 2 cm) coated glasses were washed and sonicated for 15 min in acetone, ultrapure water and ethanol, respectively; 10 mg of the photocatalyst powder was dispersed in a mixed solution containing 1 mL of ethanol and 10 μL of 10% Nafion solution and further sonicated for 30 min to obtain the well-dispersed photocatalyst suspension. Further, 100 μL of the suspension was dropped onto an FTO surface with an effective area of 1 cm × 1 cm and then dried at 60 °C. The photoelectrochemical test was probed with a three-electrode system in 50 mL 1 M Na_2SO_4 aqueous solution. Photocatalyst-loaded FTO was applied as a working electrode, a saturated calomel electrode served as a reference electrode and Pt foil was taken as the counter electrode. A 300 W Xenon lamp (Perfect light, PLS-SXE300, 100 mW/cm^2) with a long pass cut-off filter (>400 nm) was chosen as the light source. The distance between the working electrode and the filter was maintained at 10 cm.

Photoelectrochemical measurements were carried out by a CHI-760E electrochemical workstation. The transient photocurrent density of the obtained electrodes was measured using a 50-s on-off cycle with a voltage of 0.4 V under visible light (>400 nm) irradiation. Electrochemical impedance spectroscopy (EIS) tests were carried out at an open circuit potential with testing frequencies ranging from high (10^5 Hz) to low (1 Hz).

S5. AQE calculations

The apparent quantum efficiency (AQE) of Pym/S-CNNTs was determined at λ= 420 nm. After the 20 mg catalyst suspension was illuminated for 4 h, the amount of H_2 molecules generated was 6.53 μmol. The average power intensity of the incident light was measured to be 0.0348 W/cm^2 by a photometer (LPM 100/A, Coherent Inc.) and the radius of the irradiation area was 2.5 cm. The AQE was calculated from Equation (3).

$$AQE(\%) = \frac{N_e}{N_p} \times 100\% = \frac{2 \times M \times N_A \times h \times c}{S \times p \times t \times \lambda} \times 100\% \quad (3)$$

where M represents the generated H_2 molecules, N_A is the Avogadro constant (6.022×10^{23} mol^{-1}), h is the Planck constant (6.626×10^{-34} J s), and c is the speed of light (3×10^8 m s^{-1}). S, p, t, and λ are the irradiation area, intensity, time, and wavelength, respectively.

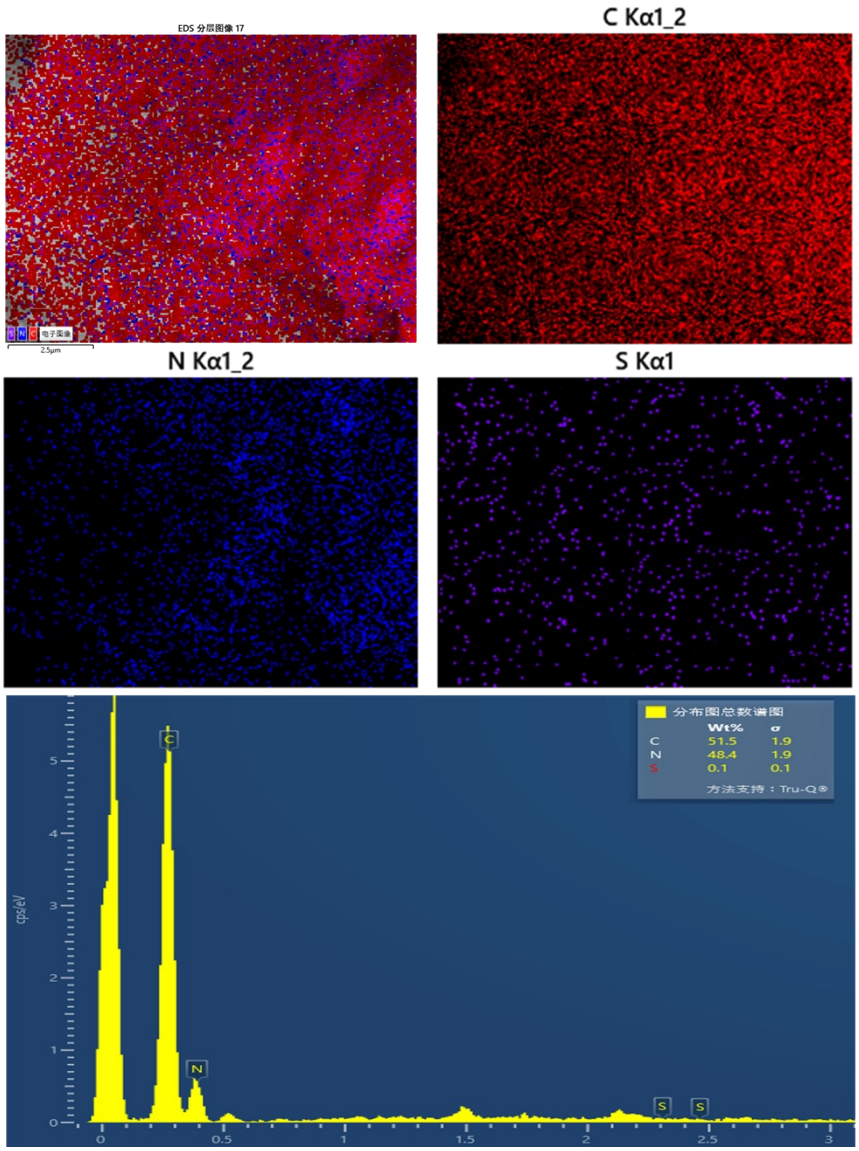

Figure S1 SEM-EDX of Pym/S-CNNTs.

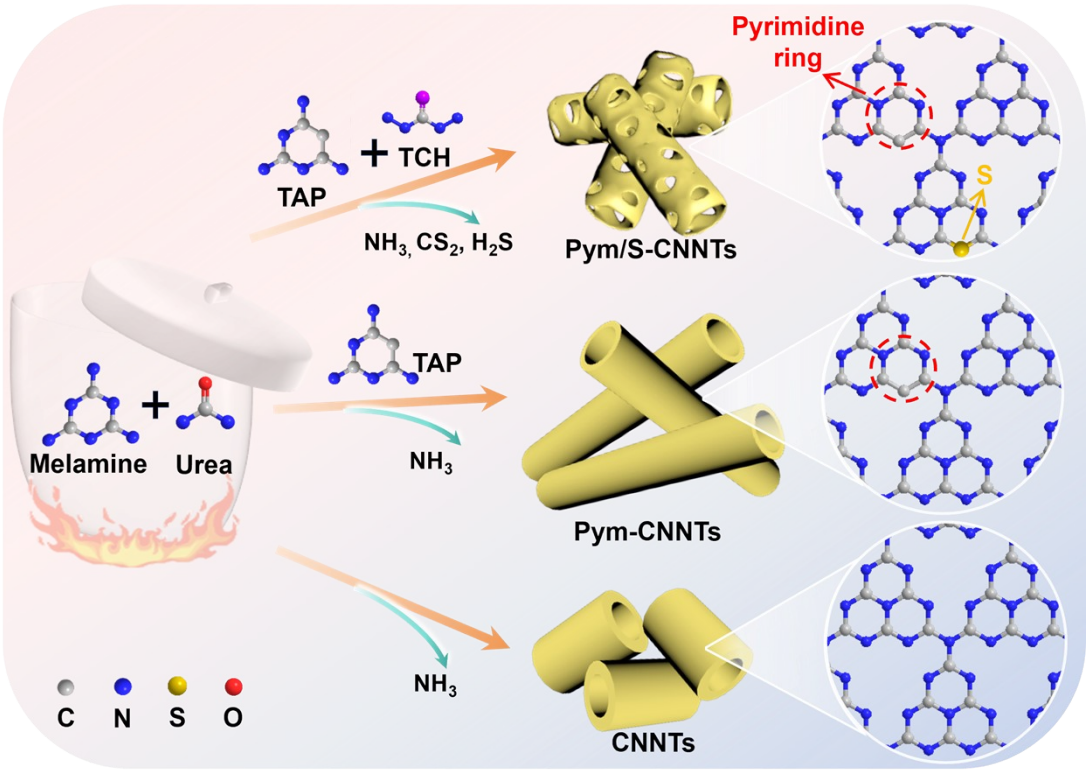

Figure S2 Schematic illustration of the catalyst preparation process.

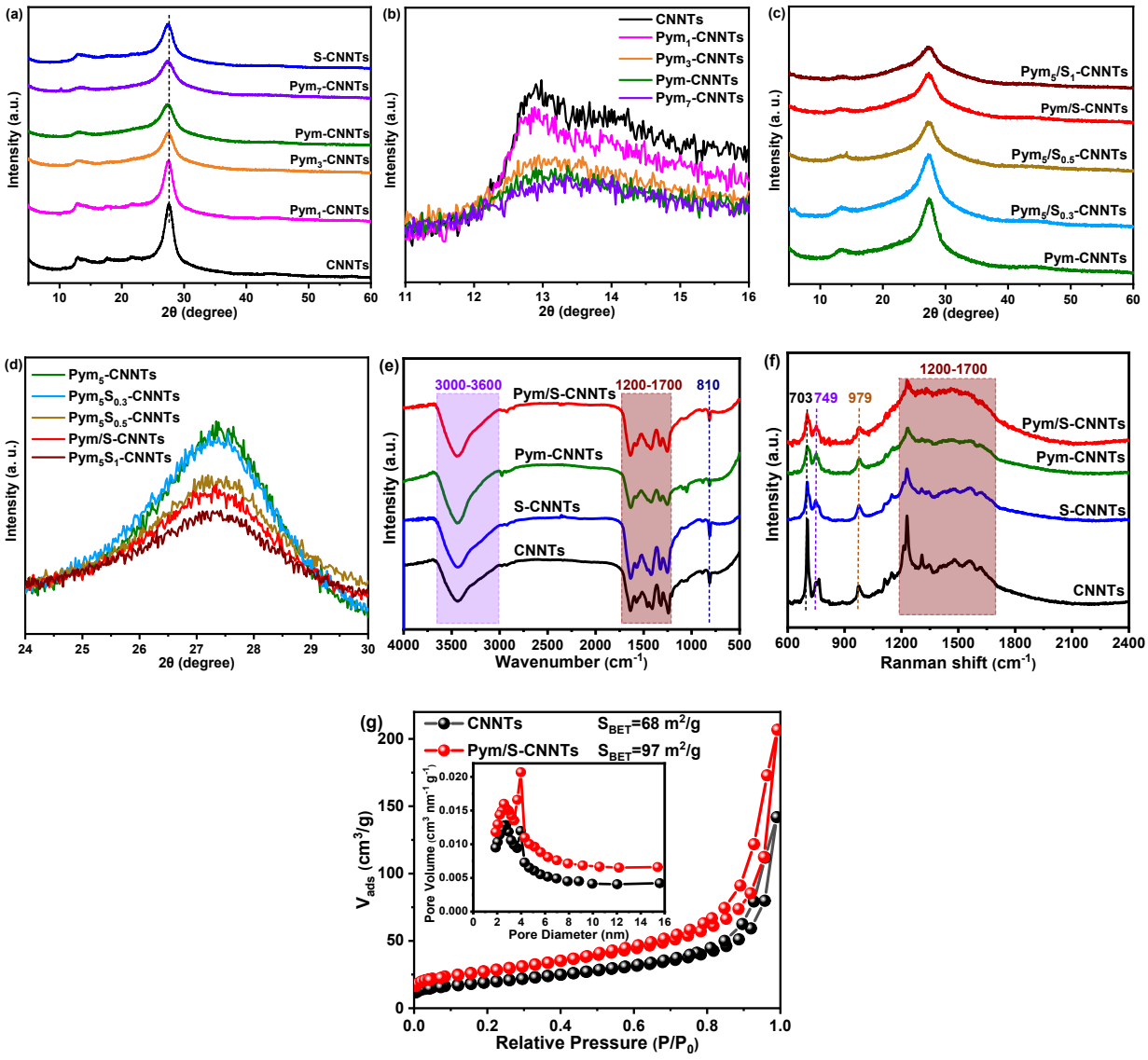

Figure S3 XRD patterns (a,b) of CNNTs, Pym_1-CNNTs, Pym_3-CNNTs, Pym-CNNTs and Pym_7-CNNTs. XRD patterns (c,d) of Pym_5-CNNTs, $Pym_5S_{0.3}$-CNNTs, $Pym_5S_{0.5}$-CNNTs, Pym/S-CNNTs and Pym_5S_1-CNNTs. FTIR (e) and Raman spectra (f) of CNNTs, S-CNNTs, Pym-CNNTs and Pym/S-CNNTs. N_2 adsorption-desorption isotherms of CNNTs and Pym/S-CNNTs (g).

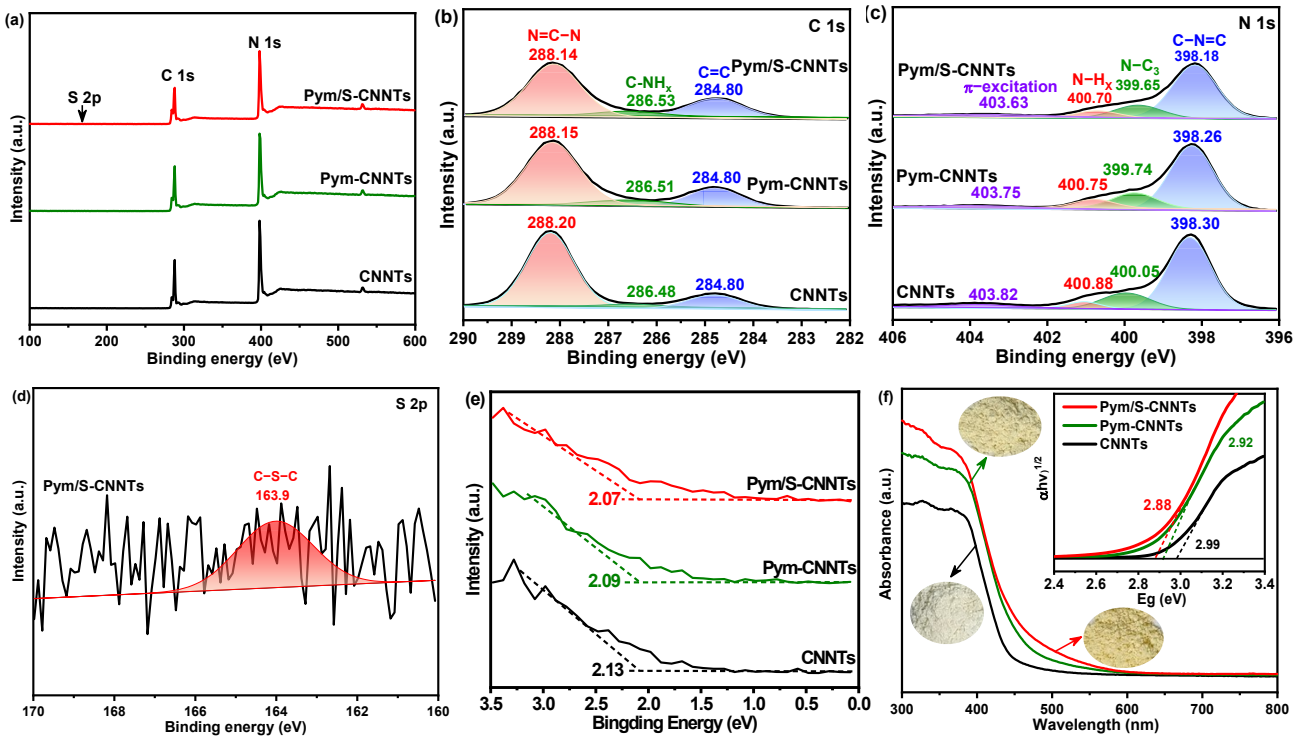

Figure S4 XPS survey spectra of CNNTs, Pym-CNNTs and Pym/S-CNNTs (a). High-resolution XPS spectra of C 1s (b) and N 1s (c) of CNNTs, Pym-CNNTs and Pym/S-CNNTs. High-resolution XPS spectrum of S 2p of Pym/S-CNNTs (d). VB-XPS of CNNTs, Pym-CNNTs and Pym/S-CNNTs (e). UV-vis DRS spectra of CNNTs, Pym-CNNTs and Pym/S-CNNTs (f).

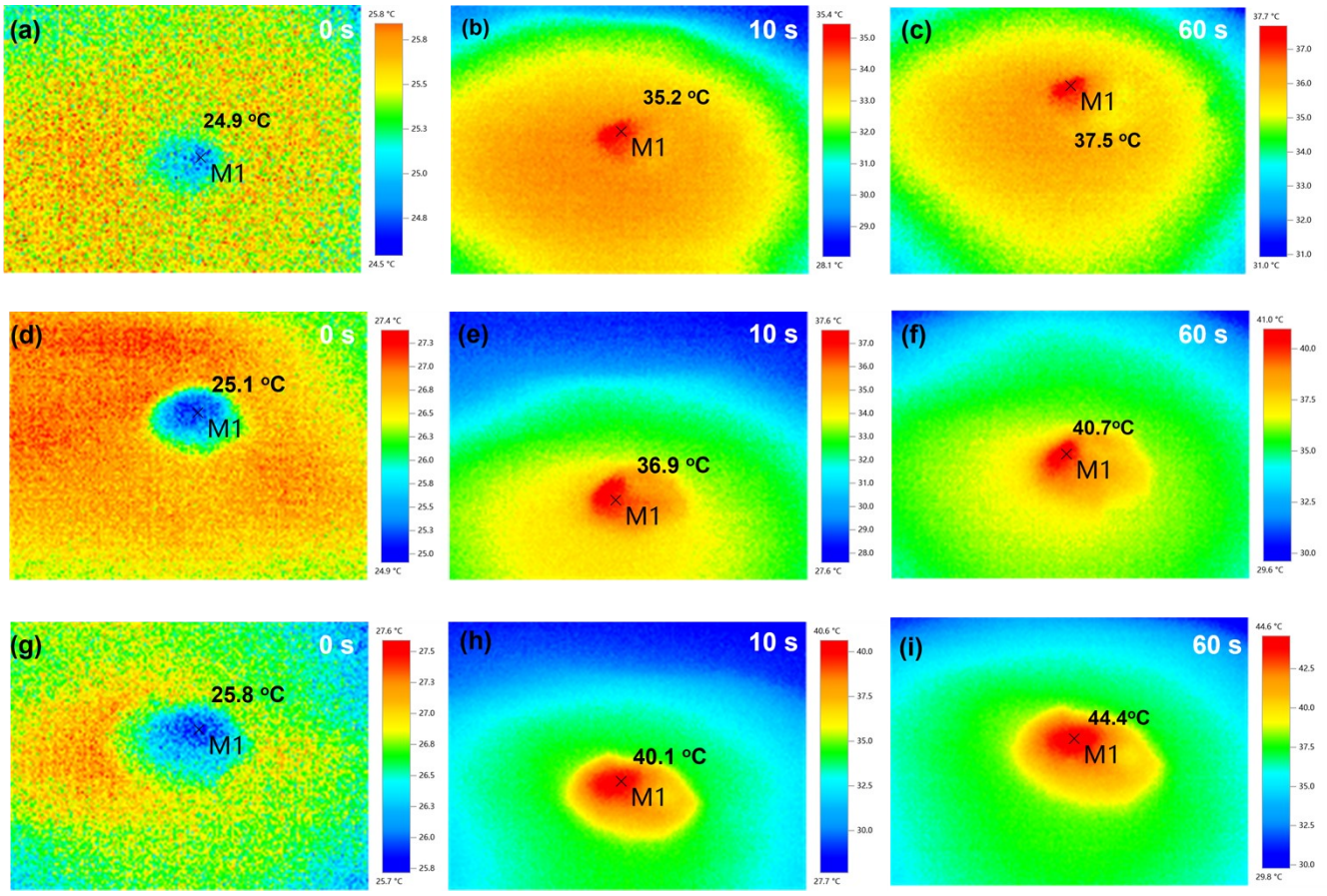

Figure S5 Time-dependent infrared images of CNNTs (a-c), Pym-CNNTs (d-f) and Pym/S-CNNTs (g-i).

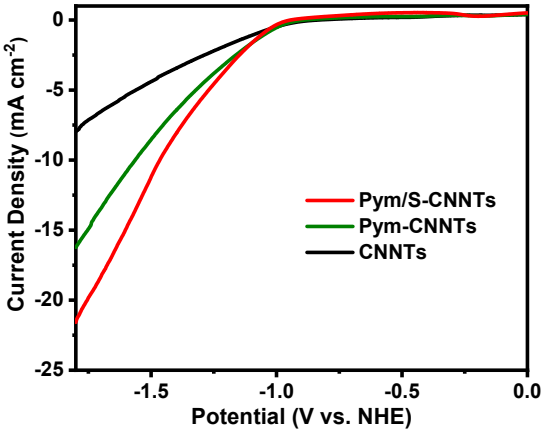

Figure S6. LSV curves of the CNNTs, Pym-CNNTs and Pym/S-CNNTs.

Figure S7 Top-down irradiation photoreactor (250 mL): front view (a), top view(b) and photocatalytic test system (c).

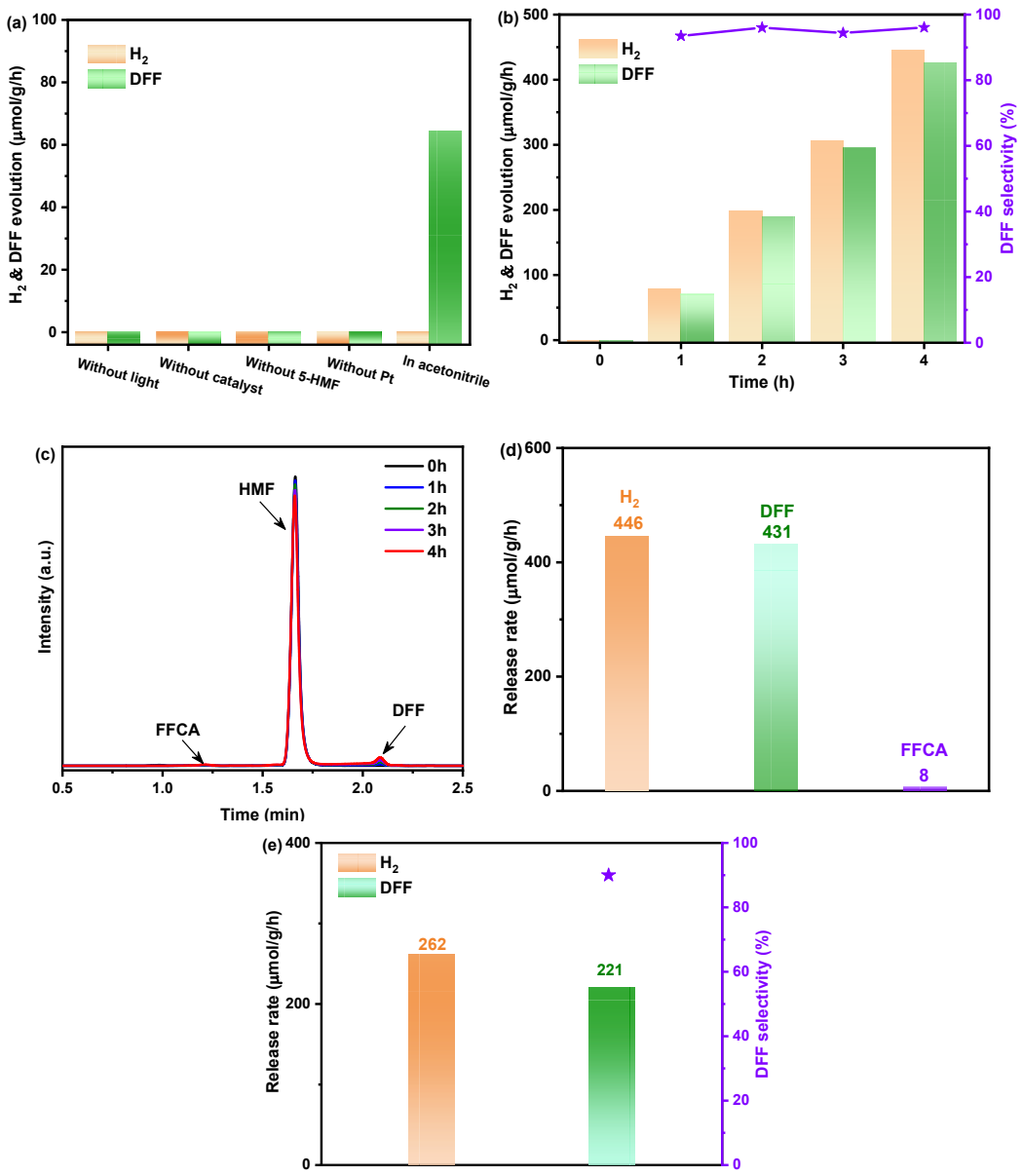

Figure S8 Photocatalytic performance for selective oxidation of HMF coupled with H_2 evolution (a,b). The HPLC spectra of the liquid products from the photocatalytic reaction over Pym/S-CNNTs at 0, 1, 2, 3 and 4 h (c). Photocatalytic synthesis of value-added chemicals from HMF over Pym/S-CNNTs (d). Photocatalytic DFF and H_2 production rates and DFF selectivity over Pym/S-CNNTs under AM 1.5G (100 mW cm^{-2}) simulated sunlight irradiation and Ar atmosphere (e).

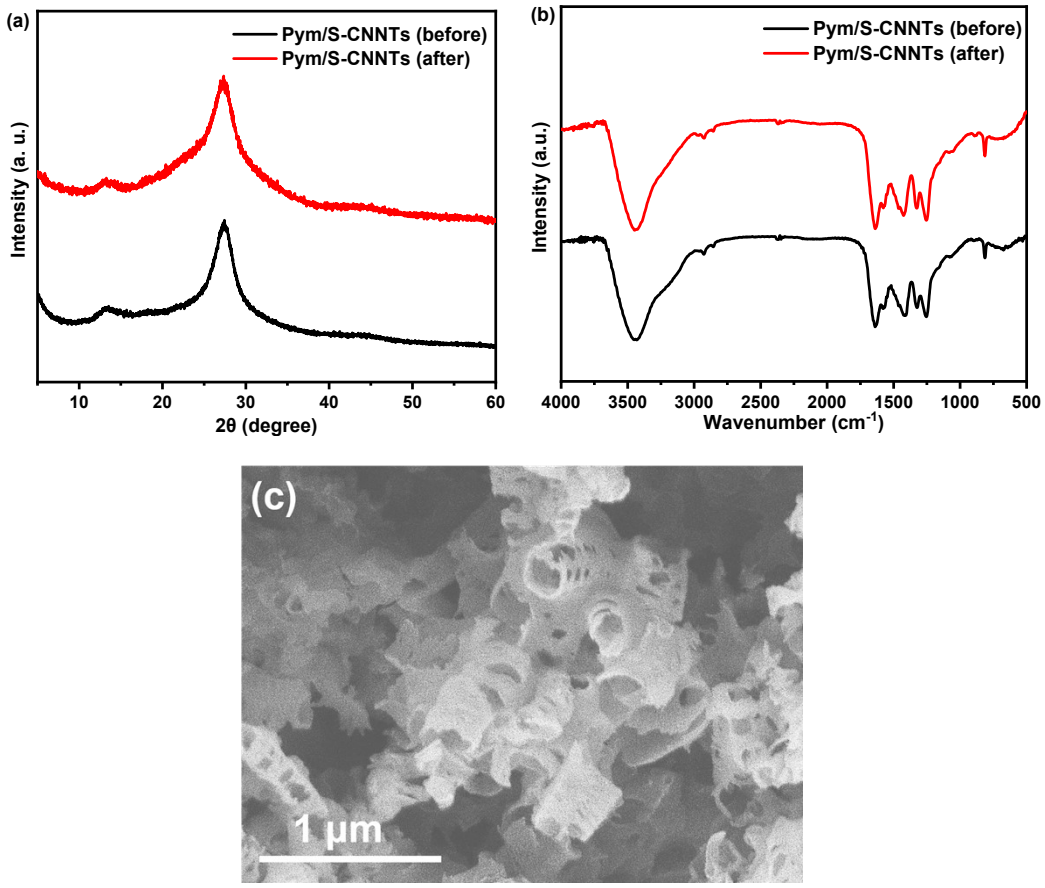

Figure S9 XRD patterns (a) and FTIR spectra (b) of Pym/S-CNNTs before and after the cycling experiments. SEM image (c) of Pym/S-CNNTs after the cycling experiments.

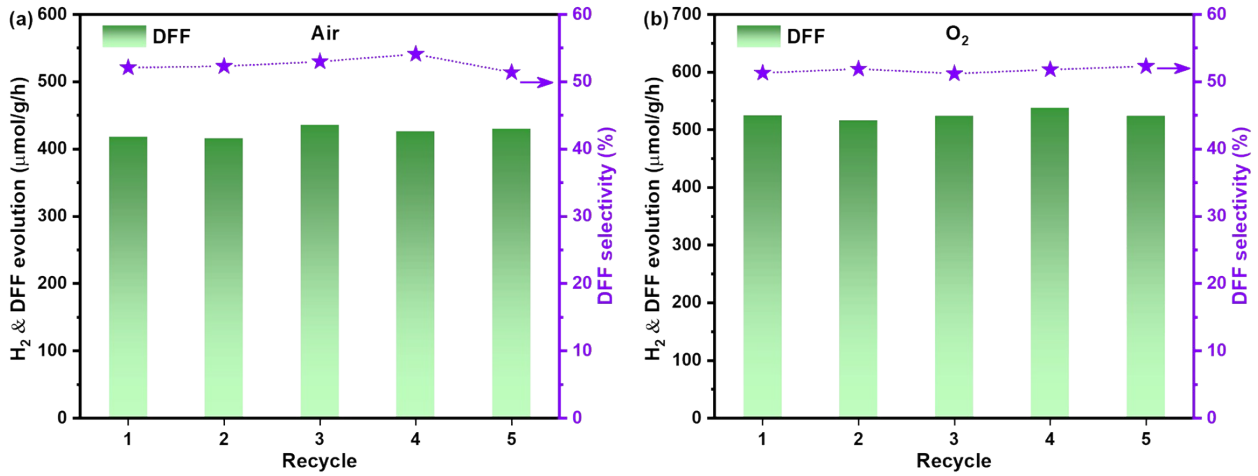

Figure S10 DFF production rates and DFF selectivity for Pym/S-CNNTs in five consecutive cycles under air (a) and O_2 atmospheres (b).

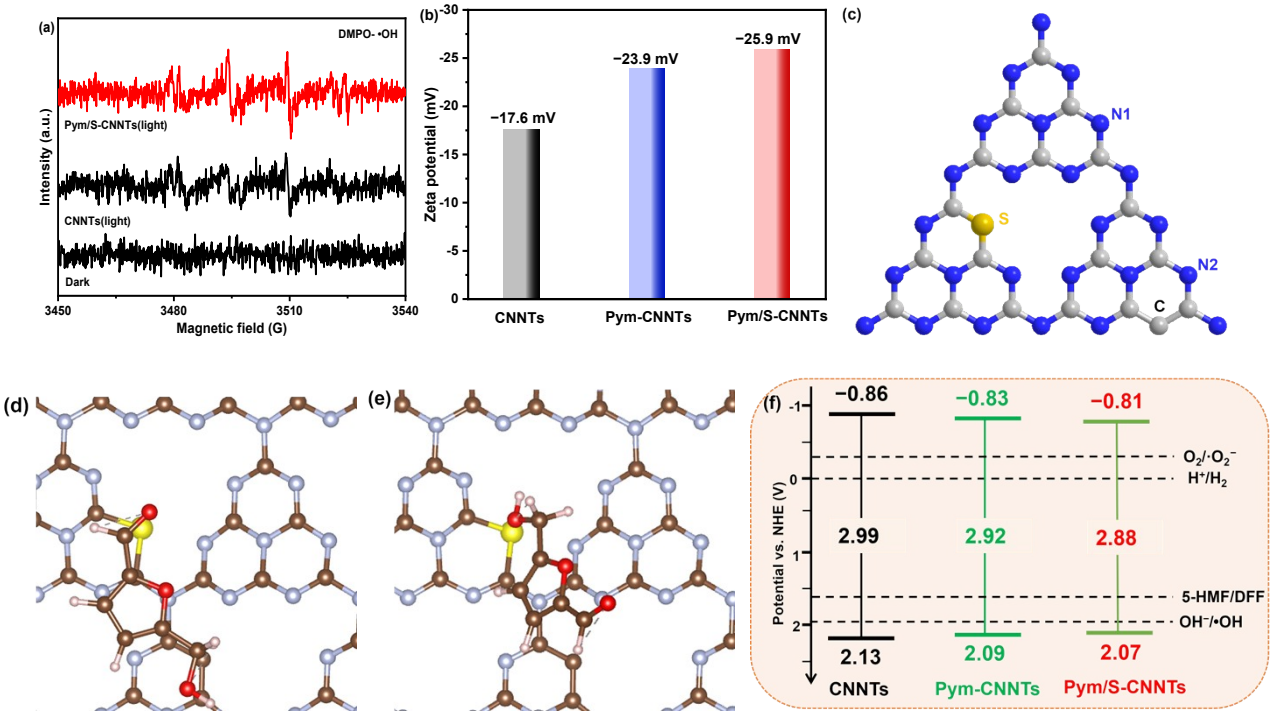

Figure S11 DMPO EPR spin-labeling of the hydroxyl radical species on CNNTs and Pym/S-CNNTs in an Ar atmosphere (a). Zeta potential of CNNTs, Pym-CNNTs and Pym/S-CNNTs (b). The selective N sites, C- and S-doped sites in Pym/S-CNNTs (c). The adsorption configurations of hydroxyl (d) and aldehyde group (e) of HMF on S site over Pym/S-CNNTs. Brown, gray, white, red, and yellow balls represent C, N, H, O, and S, respectively. The energy band structures of CNNTs, Pym-CNNTs and Pym/S-CNNTs (f).

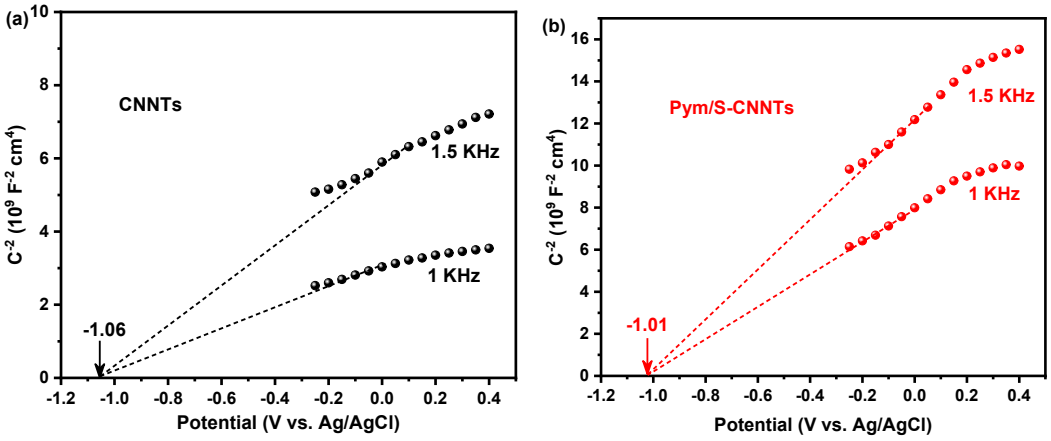

Figure S12 Mott-Schottky plots of CNNTs (a) and Pym/S-CNNTs (b).

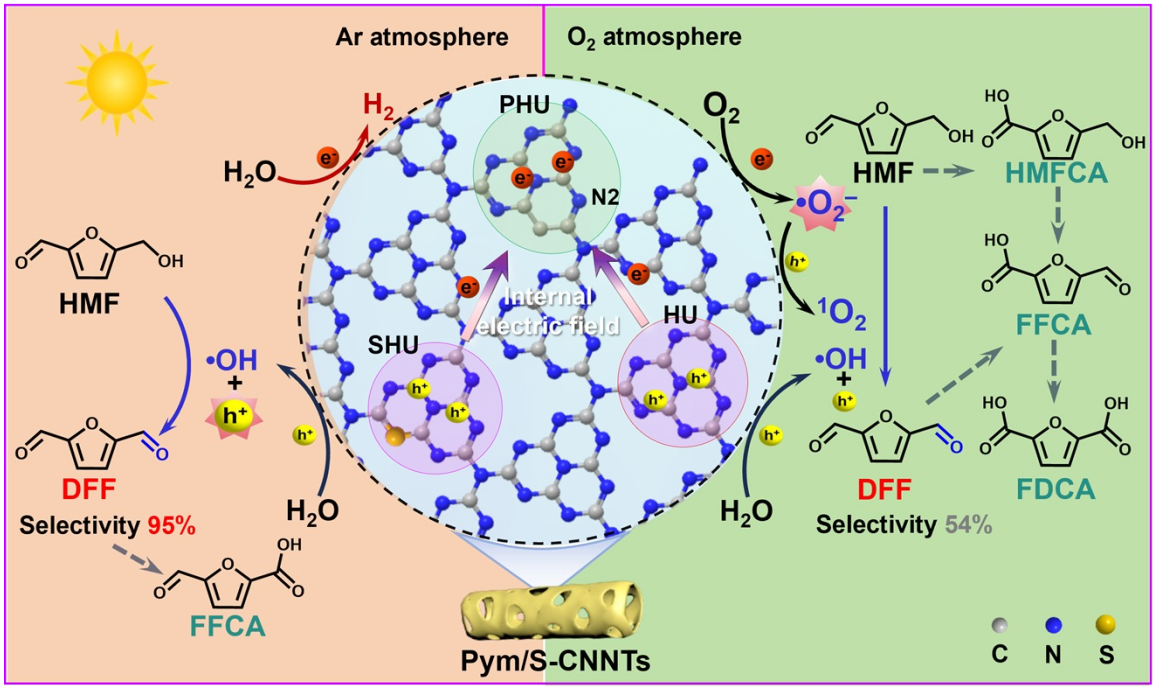

Figure S13 Possible reaction mechanism of photocatalytic HMF oxidation over Pym/S-CNNTs under Ar and O_2 atmosphere, respectively.

Table S1 Chemical compositions of the prepared samples are determined by XPS.

Samples	C (atomic%)	N (atomic%)	S (atomic%)	C/N atomic ratios
CNNTs	42.49	57.51	/	0.74
Pym-CNNTs	43.38	56.62	/	0.77
Pym/S-CNNTs	44.08	55.76	0.16	0.79

Table S2 Elemental compositions of the prepared samples are determined by elemental analysis.

Samples	C (atomic%)	N (atomic%)	S (atomic%)	H (atomic%)	C/N atomic ratios
CNNTs	36.97	51.04	/	2.14	0.72
Pym-CNNTs	39.51	51.30	/	2.55	0.77
Pym/S-CNNTs	40.23	51.39	0.19	2.05	0.78

Table S3 Quantitative XPS analysis of the deconvoluted C 1s in the resultant catalysts.

Catalyst	Deconvoluted C 1s (at %)			C=C/N–C=N
	N–C=N	C=C	C–NH_x	
CNNTs	79.28	15.73	4.99	0.20
Pym-CNNTs	70.95	19.17	9.88	0.27
Pym/S-CNNTs	70.63	23.95	5.42	0.34

Table S4 Quantitative XPS analysis of the deconvoluted N 1s in the resultant catalysts.

Catalyst	Deconvoluted N 1s (at %)			$N–(C)_3$/C–N=C
	C–N=C	$N–(C)_3$	–NH_x	
CNNTs	75.01	18.24	6.75	0.24
Pym-CNNTs	71.96	19.02	9.02	0.26
Pym/S-CNNTs	72.13	19.69	8.18	0.27

Table S5 Parameters extracted from the fitted results of EIS spectra for CNNTs, Pym-CNNTs and $C_{0.5}S_{0.7}$-CNNTs photocatalysts.

Samples	R1 (Ω)	R2 (Ω)
CNNTs	40.23	4686
Pym-CNNTs	49.89	1987
$S_{0.7}$Pym-CNNTs	63.49	1053

Table S6 The photocatalytic water splitting coupling with glucose oxidation.

Photocatalyst	Light source	H_2 evolution ($\mu mol\ g^{-1}\ h^{-1}$)	DFF yield ($\mu mol\ g^{-1}\ h^{-1}$)	DFF selectivity (%)	Ref. (Year)
Pym/S-CNNTs	300 W Xe lamp ($\lambda > 400$ nm)	446	431	~95	This work
$Ni/ZnIn_2S_4$	300 W Xe lamp ($\lambda > 400$ nm)	342	394	>97	2024 [5]
Carbon-rich CN	AM 1.5G ($\lambda > 420$ nm)	75	89	92	2024 [6]
TpPy (D-A)	Xe lamp ($\lambda > 400$ nm)	310	275	98[a]	2024 [7]
CMP-Tz (D-A)	300 W Xe lamp ($\lambda > 420$ nm)	180[a]	200[a]	~95	2023 [8]
CN-ht	AM 1.5G with an ultraviolet filter	41	49	~88	2023 [9]
NiS_2/CdS	300 W Xe lamp ($\lambda > 420$ nm)	476	519	90	2023[10]
$CoP/Zn_{0.5}Cd_{0.5}S$	300 W Xe lamp ($\lambda > 420$ nm)	598	398	87	2022 [11]
UCNT	300 W Xe lamp ($\lambda > 420$ nm)	92	95	95	2022 [12]
$NiS/Zn_3In_2S_6$	300 W Xe lamp ($\lambda > 400$ nm)	120	129	94	2020 [13]

[a] Estimated from the published photocatalytic performance curve in the literatures.

Reference

1. G. Kresse and J. J. C. m. s. Furthmüller, Efficiency of ab-initio total energy calculations for metals and semiconductors using a plane-wave basis set, Comp. Mater. Sci., 1996, 6, 15-50.
2. G. Kresse and D. Joubert, From ultrasoft pseudopotentials to the projector augmented-wave method, Phys. Rev. B, 1999, 59, 1758.
3. J. P. Perdew, K. Burke and M. J. P. r. l. Ernzerhof, Generalized gradient approximation made simple, Phys. Rev. Lett, 1996, 77, 3865.
4. M. Dion, H. Rydberg, E. Schröder, D. C. Langreth and B. Lundqvist, Van der Waals density functional for general geometries, Phys. Rev. Lett, 2004, 92, 246401.
5. S. Si, P. Gong, X. Bao, X. Tan, Y. Mao, H. Zhang, D. Xiao, K. Song, Z. Wang, P. Wang, Y. Liu, Z. Zheng, Y. Dai, B. Huang and H. Cheng, Visible-light-driven highly selective 5-hydroxymethylfurfural upgrading and H_2 generation via atomically dispersed Ni sites on $ZnIn_2S_4$ nanosheets, ACS Catal., 2024, 14, 8343-8352.
6. H.-T. Liu, T.-J. Lin, D.-L. Tsai, C.-J. Wu and J.-J. Wu, Hydroxymethylfurfural adsorption modulating charge separation characteristics of carbon-rich carbon nitrides for simultaneous photocatalytic hydrogen evolution and 2,5-diformylfuran production, Mater. Today Energy, 2024, 45, 101696.
7. Q. Yang, C. Zhang, X. Li, Y. Yuan, K. Liu, H. Cao, H. Yan and Z. Su, Donor–acceptor β-ketoenamine-based photocatalysts with a tuning band structure for selective oxidation of a biomass derivative, ACS Sustainable Chem. Eng., 2023, 12, 1951-1959.
8. Y. Yan, X. Yu, C. Shao, Y. Hu, W. Huang and Y. Li, Atomistic structural engineering of conjugated microporous polymers promotes photocatalytic biomass valorization, Adv. Funct. Mater., 2023, 33, 2304604.
9. C.-C. Chen, D.-L. Tsai, H.-T. Liu and J.-J. Wu, Carbon Vacancy-modified carbon nitride allotropic composite for solar hydrogen generation coupled with selective oxidation of 5-hydroxymethylfurfural, ACS Sustainable Chem. Eng., 2023, 11, 6435-6444.
10. S. Liu, B. Zhang, Z. Yang, Z. Xue and T. Mu, Deep eutectic solvothermal NiS_2/CdS synthesis for the visible-light-driven valorization of the biomass intermediate 5-hydroxymethylfurfural (HMF) integrated with H_2 production, Green Chem., 2023, 25, 2620-2628.
11. Y. Yang, W. Ren, X. Zheng, S. Meng, C. Cai, X. Fu and S. Chen, Decorating $Zn_{0.5}Cd_{0.5}S$ with C,N Co-doped CoP: an efficient dual-functional photocatalyst for H_2 evolution and 2,5-diformylfuran oxidation, ACS Appl. Mater. Interfaces, 2022, 14, 54649-54661.
12. X. Bao, M. Liu, Z. Wang, D. Dai, P. Wang, H. Cheng, Y. Liu, Z. Zheng, Y. Dai and B. Huang, Photocatalytic selective oxidation of HMF coupled with H_2 evolution on flexible ultrathin g-C_3N_4 nanosheets with enhanced N–H interaction, ACS Catal., 2022, 12, 1919-1929.
13. S. Meng, H. Wu, Y. Cui, X. Zheng, H. Wang, S. Chen, Y. Wang and X. Fu, One-step synthesis of 2D/2D-3D NiS/$Zn_3In_2S_6$ hierarchical structure toward solar-to-chemical energy transformation of biomass-relevant alcohols, Appl. Catal. B Environ., 2020, 266, 118617.